PLASMA MORPHOLOGY AT MARS. ASPERA-3 OBSERVATIONS

E. DUBININ[1,*], M. FRÄNZ[1], J. WOCH[1], E. ROUSSOS[1], S. BARABASH[2],
R. LUNDIN[2], J. D. WINNINGHAM[3], R. A. FRAHM[3] and M. ACUÑA[4]

[1]*MPI für Sonnensystemforschung, 37191 Katlenburg-Lindau, Germany*
[2]*Swedish Institute of Space Physics, Kiruna, Sweden*
[3]*Southwest Research Institute, San-Antonio, USA*
[4]*NASA Goddard Space Flight Center, Greenbelt, USA*
(*Author for correspondence: E-mail: dubinin@mps.mpg.de)

Abstract. A total of about of 400 orbits during the first year of the ASPERA-3 operation onboard the Mars Express spacecraft were analyzed to obtain a statistical pattern of the main plasma domains in the Martian space environment. The environment is controlled by the direct interaction between the solar wind and the planetary exosphere/ionosphere which results in the formation of the magnetospheric cavity. Ionospheric plasma was traced by the characteristic "spectral lines" of photoelectrons that make it possible to detect an ionospheric component even far from the planet. Plasma of solar wind and planetary origin was distinguished by the ion mass spectrometry. Several different regions, namely, boundary layer/mantle, plasma sheet, region with ionospheric photoelectrons, ray-like structures near the wake boundary were identified. Upstream parameters like solar wind ram pressure and the direction of the interplanetary electric field were inferred as proxy from the Mars Global Surveyor magnetic field data at a reference point of the magnetic pile up region in the northern dayside hemisphere. It is shown that morphology and dynamics of the main plasma domains and their boundaries are governed by these factors as well as by local crustal magnetizations which add complexity and variability to the plasma and magnetic field environment.

Keywords: Mars: magnetosphere, Mars: ionosphere, sun: solar wind

1. Introduction

Previous missions to Mars have established the existence of the main plasma regions near Mars. Mariner 4 which passed within $3.9R_M$ of Mars in 1965 has detected a bow shock. At the bow shock, solar wind is deflected around the Martian obstacle. However, as the previous spacecraft (except the Viking landers which have not carried an onboard magnetometer) have not approached Mars closer than $\sim$850 km, the nature of the obstacle to the solar wind was not finally resolved before the Mars Global Surveyor (MGS) mission. The MGS measurements have shown that at present Mars does not possess a global intrinsic magnetic field which could be an obstacle for the solar wind as for most of other planets in our solar system (Acuña *et al*., 1998). Instead, MGS has detected localized, rather strong magnetic anomalies of a crustal origin. Due to the absence of a magnetic obstacle at Mars the solar wind directly interacts with its upper atmosphere and ionosphere and induces a magnetosphere by the pile up of the interplanetary magnetic field. Such an induced

magnetosphere can screen the ionosphere from the direct exposure to the solar wind. The formed magnetic barrier separates the solar wind from the ionosphere and acts as an effective obstacle deflecting the magnetosheath plasma.

A similar type of interaction occurs around another nonmagnetized planet, Venus, and was extensively explored by the Pioneer-Venus-Orbiter in over 14 years of operation (see, for example, Russell, 1992). Although the PVO mission has provided a wealth of excellent in-situ data about the solar wind/ionosphere interaction for a wide range of solar wind conditions, the plasma ion component in the energy range ∼10 eV–10 keV was studied rather poorly because of instrument and telemetry constraints. The MGS science payload does not include a plasma instrument for the measurement of ion components at Mars, and therefore only the MEX mission and the ASPERA-3 in-situ measurements fill this gap (curiously, there is no magnetometer on MEX).

It is also worth noting that active comets interacting with solar wind develop similar plasma field and magnetic structures as Mars or Venus (Slavin *et al*., 1986; Neubauer, 1987; Raeder *et al*., 1987; Mazelle *et al*., 1989).

The most convincing evidence of the formation of the magnetic barrier at Mars was the observations of the magnetic pile up boundary (MPB), a sharp boundary with a strong jump in the magnetic field strength, a drop in the magnetic field fluctuations and a strong decrease in the superthermal electron fluxes (Acuña *et al*., 1998). According to Bertucci *et al*. (2003) the MPB is also characterized by an increase in the magnetic field line draping. Downstream from the MPB, a region called the magnetic pile up region (MPR) is characterized by a sustained high magnetic field. It was believed, despite of a lack of ion measurements on MGS, that the MPB separates the region of shocked solar wind (magnetosheath) from the induced magnetosphere. Such an assumption was supported by the Phobos-2 observations (Breus *et al*., 1991; Pedersen *et al*., 1991; Dubinin *et al*., 1996). It will be shown subsequently that, indeed, a magnetospheric cavity almost void of the solar wind plasma is formed at Mars.

There is also a somewhat different view. Mitchell *et al*. (2001) have suggested that another boundary, "ionopause," observed at lower altitudes separates ionospheric and solar wind plasmas. This boundary was detected by the comparison of electron spectra, with magnetosheath-like solar wind electrons above the boundary and ionospheric photoelectrons below the boundary. Its median altitude at solar zenith angles (SZAs) of about 80° was estimated as 380 km. In between, Mitchell *et al*. (2001) identified a "transition region" which the authors compare with the Venusian plasma mantle whose the lower boundary is the ionopause (Spenner *et al*., 1980). Recall that the term ionopause was introduced to describe the direct interaction between the solar wind plasma and ionosphere at Venus. The currents flowing in the thin layer (ionopause), where the external hot solar wind magnetized plasma and cold ionospheric plasma balance each other, screen the magnetic field from the ionosphere. They cause a pileup of magnetic field lines in front of the ionopause. A magnetic field barrier of piled up field lines almost balances the solar wind pressure.

On the other hand, the magnetic field pressure balances the thermal ionospheric pressure at lower altitudes. As a result, the real obstacle to the solar wind is observed at the magnetic barrier whose position is further from the planet than the ionopause (see, for example, Zhang *et al*., 1991). If the ionosphere is resistive the ionopause is broadened and the magnetic field penetrates deeper into the ionosphere. This happens, for example, when the solar wind pressure increases and the ionopause moves to lower altitudes where there are more collisions between particles.

However, as it will be shown in this paper, a stoppage of the solar wind at Mars occurs at higher altitudes, at the boundary, identified earlier as MPB.

The Martian ionosphere, formed by the photoionization of the major neutral constituents CO_2 and O with subsequent molecular reactions giving rise to O_2^+ as the major ionospheric ion species and O^+ becoming comparable at altitudes ≥ 300 km is poorly explored as compared to Venus. The measurements of the main ionospheric characteristics at Mars were made in-situ by the two Viking landers (Hanson *et al*., 1977; Hanson and Mantas, 1988), that provided us with two ionospheric height profiles, and by radio occultation experiments (Kliore, 1992). Recently new radio occultation and sounding measurements were carried out onboard the MEX spacecraft (Pätzold *et al*., 2005; Gurnett *et al*., 2005). Most of the radio occultation profiles show a relatively extended ionosphere without clear ionopause structure. On the other hand, a decrease in the magnetic field value within the ionosphere observed by MGS (Acuña *et al*., 1998) is a typical feature of the ionopause.

In the ASPERA-3 data, ionospheric plasma is well traced by the characteristic "spectral lines" of photoelectrons which are resolved due to a high energy resolution of the electron spectrometer (Lundin *et al*., 2004; Frahm *et al*., 2006a,b). It will be shown here that ionospheric electrons are observed in a wide range of altitudes and the boundary of the photoelectrons (PEB) is often located at higher altitudes than it was reported by Mitchell *et al*. (2001) (see also Frahm *et al*., 2006b). It is not clear yet whether PEB and ionopause are collocated since the lowest energy part of the plasma distribution which primary contributes to the thermal pressure has not been measured yet.

It is worth noting that the region below the MPB remains a mysterious one. It will be subsequently shown that the main fluxes of escaping planetary ions are clustered in this region. Energy characteristics of ion beams yield an estimate of electric fields responsible for ion energization. The values of electric field are close to the typical values of the interplanetary motional electric field that implies an effective penetration of solar wind electric field deep into the magnetosphere and effective scavenging of planetary ions (Dubinin *et al*., 2006a).

The induced magnetosphere contains several different subregions. The boundary layer/mantle dominated by planetary plasma was identified in the previous missions (Vaisberg, 1992; Lundin *et al*., 1990a; Dubinin *et al*., 1996). This boundary layer can be considered as a site where the momentum of the solar wind is transferred to the planetary plasma (Lundin *et al*., 1991; Lundin and Dubinin, 1992). Ray-like structures stretched in the tailward direction were measured on Phobos-2 as well

as on the MEX spacecraft (Dubinin *et al*., 2001, 2006b). It is shown in this paper that both these regions, namely, the boundary layer and plasma rays are important channels for transportation of planetary ions to the tail.

The magnetotail of Mars consists of two lobes of opposite polarity separated by plasma sheet (Yeroshenko *et al*., 1990). The plasma sheet consists primarily of planetary ions which are accelerated up to keV energies by the magnetic field tensions (Dubinin *et al*., 1993). The Phobos-2 observations in the tail at distances of $\sim 2.8 R_M$ from the planet have revealed signatures of field lines of crustal origin (Dubinin *et al*., 1994) that implies a complicated magnetic structure of the tail due to reconnection of the IMF and crustal field lines. Large-scale modification of the plasma flow in the tail due to the crustal field contribution was observed in 3D-MHD simulations (Harnett and Winglee, 2005).

Crustal fields add complexity and variability to the Martian magnetic environment (Brain *et al*., 2003, 2006). The strongest crustal source was detectable up to altitudes of 1300–1400 km and, as it will be shown subsequently, it shifts the magnetospheric boundary upwards (see also Crider, 2004; Fraenz *et al*., 2006a). To date it is not clear whether the local crustal fields are able to balance the thermal pressure of the magnetosheath plasma or the upward motion of the magnetospheric boundary occurs due to local ionospheric inflations caused by a lift of the ionospheric electrons. The crustal field also shields the localized regions from intrusion of the magnetosheath plasma (minimagnetospheres) (Brain *et al*., 2005; Fraenz *et al*., 2006a).

In this paper we have analyzed about 400 orbits during the first year (Feb.–Dec. 2004) of the ASPERA-3 operation onboard the Mars Express spacecraft. In some cases, when we did not use an information about the upstream solar wind and IMF parameters, we have analyzed the observations of two years (2004–2005). MEX ASPERA-3 data provide information about the main plasma domains of the Martian space environment. We present an analysis of the morphology of these regions and their boundaries. We analyze the MGS data to infer the upstream parameters, namely, ram pressure of the solar wind and the direction of cross flow component of the IMF. We then explore the influence of these parameters on the plasma distribution within the magnetosphere and the position of boundaries. The influence of crustal sources is also studied.

2. Observations

The Mars Express spacecraft was inserted into an elliptical orbit around Mars in January 2004. This eccentric elliptical orbit has a periapsis altitude of about 275 km, an apoapsis of about 10000 km, an orbital inclination of 86° and a period of 6.75 h. The scientific payload includes the ASPERA-3 instrument with several sensors to measure electrons, ions and energetic neutral atoms (ENAs). The ASPERA-3 (Analyzer of Space Plasma and Energetic Atoms) experiment is a combination of

in-situ and remote diagnostics of atmospheric escape induced by the solar wind. It comprises the Ion Mass Analyzer (IMA), ELectron Spectrometer (ELS), Neutral Particle Imager (NPI) and Neutral Particle Detector (NPD) (Barabash *et al.*, 2004). In this paper we discuss the results obtained from the IMA and ELS sensors. The IMA sensor measures 3D-fluxes of different ion species with m/q resolution (m and q are respectively mass and electric charge) in the energy range 10 eV/q– 30 keV/q with a time resolution of ∼3 min and a field of view of $90° × 360°$ (electrostatic sweeping provides elevation coverage $±45°$). Mass (m/q) resolution is provided by a combination of the electrostatic analyzer with deflection of ions in a cylindrical magnetic field set up by permanent magnets. The ELS instrument measures 2D distributions of the electron fluxes in the energy range 0.4 eV–20 keV ($δE/E = 8\%$) with a field of view of $4° × 360°$ and a time resolution of ∼4 s. In many cases the grid biased at $−5$ V cuts the low energy ionospheric electrons. A spacecraft potential which is usually positive in solar wind and magnetosheath and negative in a dense ionosphere also strongly influences the measurements in the low energy part of the distribution function. The bulk parameters of plasma were obtained by using algorithms discussed in (Fraenz *et al.*, 2006b).

Figure 1 shows spectrograms of the electron fluxes measured by ASPERA-3 and describing the different domains of the Martian plasma environment. The dotted curves depict the altitude of the spacecraft over the Mars surface. The respective scale in km is given on the right vertical axes. The corresponding MEX orbits in cylindrical coordinates (with the X-axis directed from the Mars center towards the Sun and the radial distance R taken from the X-axis) are shown in Figure 2. In all these cases the spacecraft subsequently crossed the bow shock, magnetosheath, entered the magnetosphere and moving further along the outbound leg of the orbits recorded all these characteristic regions in the opposite order. The nominal positions of the bow shock (BS) and the magnetic pile-up boundary (MPB) (which can also be referred to as the boundary of the induced magnetosphere, MB), determined from Mars Global Surveyor (MGS) measurements (Vignes *et al.*, 2000) are also given. Pile up of the IMF accompanied by a drop of the solar wind electrons was observed at the MPB (Acuña *et al.*, 1998).

The magnetosheath region bounded by the BS and MPB is well displayed in Figure 1 by the appearance of solar wind electrons heated at the bow shock. The cavity void of magnetosheath electrons (the top panel) tells us about the existence of a magnetospheric obstacle to the solar wind. Since Mars has no global intrinsic field the magnetosphere is formed by the pile up of the interplanetary magnetic field (IMF), carried by the solar wind, and a draping of the field lines around the ionospheric obstacle. Indeed, the electron spectra within the Martian magnetosphere contain clear signatures of the ionosphere. The peaks in the electron fluxes near ∼20–30 eV appear due to the absorption of the strong solar He II line at 304 Å in the carbon dioxide dominated atmosphere of Mars (Mantas and Hanson, 1979; Frahm *et al.*, 2006a). These peaks can be used for tracing of ionospheric photoelectrons. The interesting feature is that photoelectrons are often observed not only near the
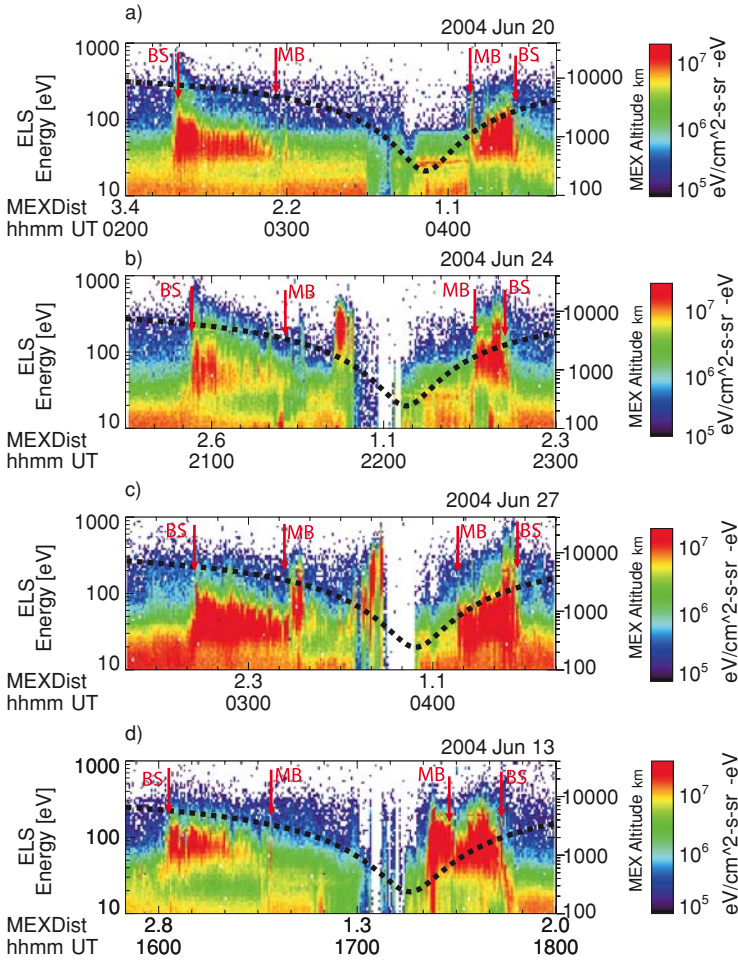
Figure 1. Spectrograms of electron fluxes along the several similar MEX orbits. Dotted curves show the MEX altitude (scale in km is given on the right vertical axis). Positions of the bow shock (BS) and magnetospheric boundary (MB) are marked by arrows.

periapsis, but also near the magnetospheric boundary. For example, ionospheric signatures are seen at an altitude of about ∼900 km, close to the MB on the outbound leg (∼0408 UT June 20, 2004). Moreover, traces of CO_2 photoelectrons are detected at much higher altitudes, up to ∼5000 km (∼0300 UT) close to the inbound MB. The thick blue segments along the MEX orbit in Figure 2 depict the region where the photoelectrons were observed. In most cases a gap (small or large) exists between the MB identified by a drop of the sheath electrons and the photoelectron boundary (PEB). The presence of this gap clearly shows that MB (or MPB) and PEB are indeed two distinct boundaries.
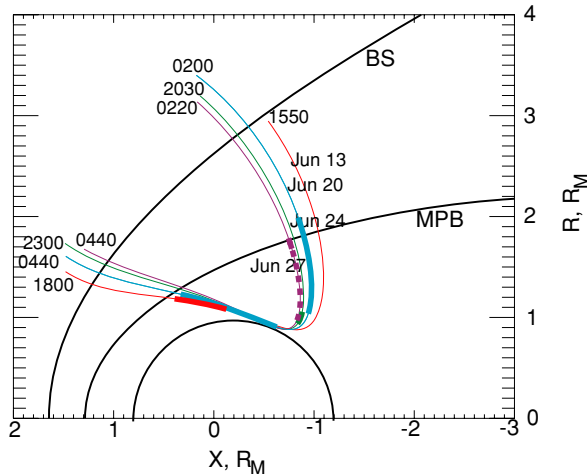
Figure 2. Orbits of MEX in cylindrical coordinates. The spacecraft enters the magnetosphere at $X \sim -1 R_M$ and exits at the dayside. The thick color segments show the location of different plasma domains discussed in the text.

New features in the electron fluxes appear within the magnetosphere on the panel (b) of Figure 1. A spatially narrow plasma structure composed of magnetosheath-like electrons is observed near the wake boundary i.e. the boundary of the geo-metrical shadow ($\sim$2150 UT and the thick green orbital segment in Figure 2). The peak energy of the electrons exceeds their peak-energy at the BS. Plasma in such structures is primarily of planetary origin (O^+ and O_2^+ ions). Different mechanisms were discussed (Dubinin *et al.*, 2006b) to explain the appearance of such structures. One scenario assumes the existence of efficient plasma transport channels into the magnetosphere in magnetic polar regions. In this description the position of the equatorial plane is controlled by the IMF direction, the equatorial plane contains the solar wind velocity and the IMF vector in the undisturbed solar wind. The mag-netic field tensions of the draped field lines which become dominant near the MPB (Bertucci *et al.*, 2003) accelerate plasma in the polar regions and push it into the magnetosphere. Such a mechanism suggests a gradual formation of a plasma sheet which separates the two magnetic tail lobes. According to another possible mech-anism, reconnection between the crustal and draped IMF field lines can open the inner magnetospheric regions up to solar wind electrons. As a result, magnetic field configurations with "auroral field lines" similar as at Earth, may appear (Lundin *et al.*, 2006).

The narrow structures near the wake boundary stretching in the tailward direc-tion are similar to rays, composed of escaping suprathermal ionospheric O^+ ions, observed at Venus (Brace *et al.*, 1987). Luhmann (1993) suggested that these struc-tures appeared from a thin source region around the terminator where the solar wind convection electric field penetrates into the oxygen-dominated high altitude

terminator ionosphere. Dubinin *et al.* (1991) have also observed such structures in the Martian tail. Most of the events were centered near the wake boundary.

On some orbits, an additional appreciable heating of the sheath electrons is observed in the region adjacent to the MB (the panel (c) in Figure 1, $\sim$0315 UT). The location of this narrow region is marked in Figure 2 by the thick violet segment. Ion composition measurements show that the plasma in such structures consists of planetary O^+ and O_2^+ ions. The top panel in Figure 3 presents the spectrogram of He^{++} and O^+ ions. Alpha-particles are used as tracers of the solar wind plasma while oxygen ions have a planetary origin. Planetary ions occupy a broad boundary layer marked in Figure 2 by the dotted violet segment. A similar, although not so appreciable structure is seen on the panel (b) at $\sim$2130 UT. The bottom panels in Figure 3 depict the normalized to the solar wind conditions number densities of electrons, protons, atomic (O^+) and molecular (O_2^+) oxygen ions, and electron temperature. Electron heating and a density increase associated with the appearance of planetary ions near the magnetospheric boundary (MB) at 0312 UT is observed. Another feature observed at $\sim$0340, near the wake boundary, is a ray structure similar to one seen on the panel (b). Note that the cutoff of the low energy ionospheric electrons strongly reduces the measured electron number densities at low altitudes.

A change of the ion composition in the boundary layer/mantle is the characteristic feature of the transition. Similar observations by the Phobos-2 spacecraft have suggested that the magnetospheric boundary at Mars is also the ion composition boundary to emphasize a sharp transition from the solar wind to planetary plasma. As a matter of fact, all these boundaries at a macroscopic scale are collocated (Dubinin *et al.*, 1996; Nagy *et al.*, 2004).

Pioneer-Venus-Orbiter observations made at another nonmagnetized planet, Venus, have shown the existence of a boundary layer with enhanced wave activity (Perez-de-Tejada *et al.*, 1993). Its appearance was attributed to a "friction" action between the shocked solar wind and planetary plasma (Perez-de-Tejada, 1979). According to Perez-de-Tejada (1993) this so-called "intermediate transition" is characterized by a decrease in the magnetic field which is not the case of the MPB/MB. Although the terms "viscosity" and "friction" are not well determined in a collisionless plasma, dissipative processes associated with the transport of the solar wind momentum to the planetary plasma could be responsible for the observed electron heating.

The panel (d) in Figure 1 demonstrates the existence of a boundary layer with an additional heating of magnetosheath electrons on the outbound leg of the orbit ($\sim$1725 UT) when the spacecraft crossed the near terminator MB. The location of the layer is marked in Figure 2 by the red orbital segment. Figure 4 presents the normalized number densities of electrons, protons, atomic (O^+) and molecular (O_2^+) oxygen ions, and the electron temperature. Note here, that the boundary layer (mantle) composed of planetary ions is not always accompanied by appreciable electron heating as for the outbound crossing (1832 UT) (see, for example, the inbound crossing at 1632 UT). The inconsistency between the electron and ion
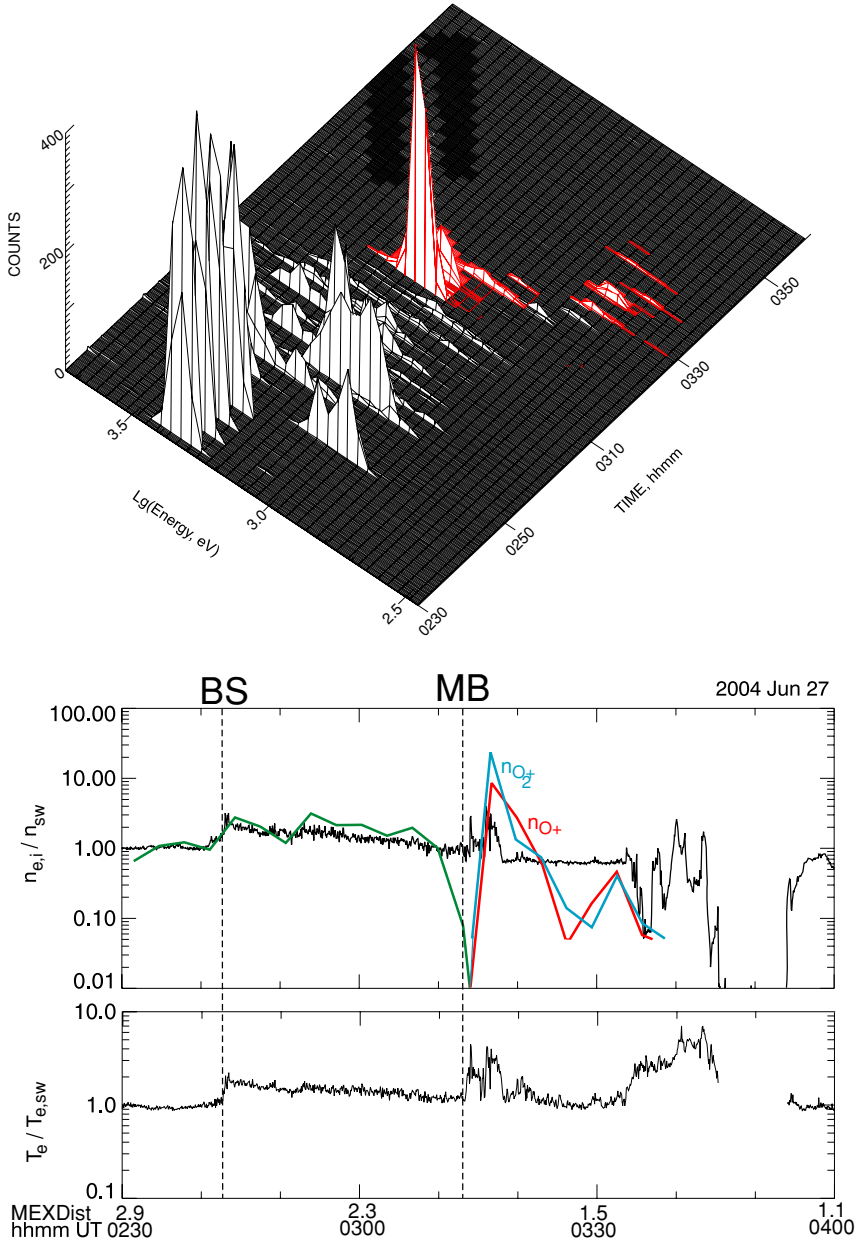
Figure 3. From top to bottom: Spectrograms of He^{++} (the black curves) and O^+ (the red curves) ions along the MEX trajectory on June 27, 2004. The oxygen ions dominate in the boundary layer/mantle adjacent to the MB crossed at ~0312 UT. Variations of the densities of the electrons (the black solid curve), protons (green curve), O^+-ions (red curve), O_2^+ ions (blue curve) and the electron temperature. The parameters for the electrons and proton are normalized to the their upstream solar wind values. Note that the electron measurements are carried out at $E_e > 5\,eV$ (repelling grid). The spacecraft potential also shifts the measured electron distribution.
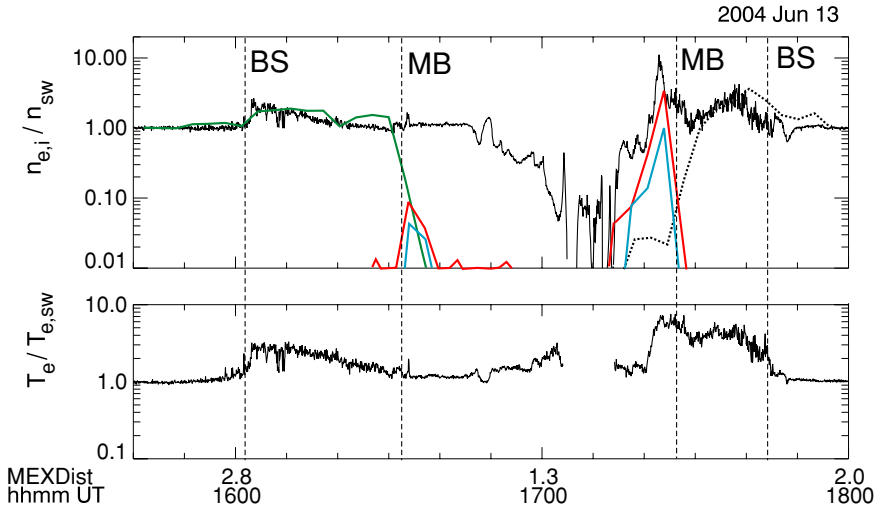
Figure 4. The normalized bulk parameters of the electrons and ions along the orbit on June 13, 2004.

number densities in the inbound magnetosphere (after 1632 UT) is due to the instrumental "gaps" in the measurements of the low-energy parts of the electron and ion distributions.

The above examples display the different characteristic features of the main plasma regions which were used to trace and explore their morphology.

2.1. MAGNETOSPHERIC BOUNDARY

We have analyzed the position of the magnetospheric boundary characterized by a drop of the magnetosheath electrons using MEX-ASPERA-3 data from February 2004–December 2004. Figure 5 presents the position of the boundary crossings plotted in cylindrical coordinates. Superposed on the data points red and blue curves depict the position of the bow shock and magnetic pile up boundary from Vignes *et al.* (2000) (MGS data) and the bow shock and planetopause (PP) from Trotignon *et al.* (1996) (Phobos-2 data), respectively. Different names of boundaries introduced from single instrument observations, as a matter of fact, correspond to the same and one magnetospheric boundary (Dubinin *et al.*, 1996; Nagy *et al.*, 2004). It is observed that at small solar zenith angles (SZAs) the position of the boundary is closer to the planet and in a better agreement with the PP position derived from the Phobos-2 measurements although the solar activity during these missions was very different (Figure 6). In contrast, at larger SZAs, the positions of the MB and MPB are in a reasonable agreement. The difference between two model curves is not statistically significant since the vast majority of the Phobos-2 crossings of the MB was at the night side, and a lack of the MGS measurements at low SZAs.
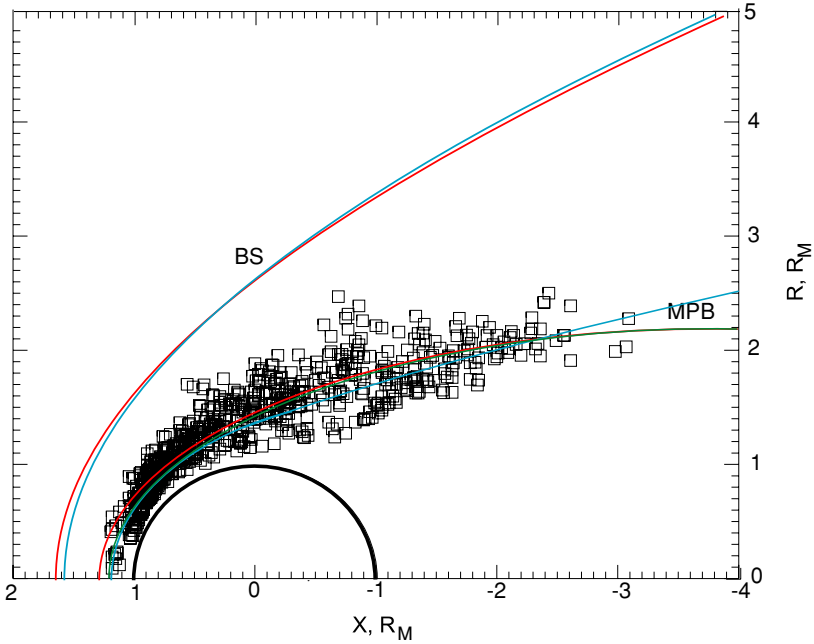
Figure 5. Positions of the magnetospheric boundary in cylindrical coordinates. Red and blue curves depict the nominal positions of the bow shock (BS) and the magnetospheric boundary inferred from the MGS and Phobos-2 observations, respectively. The green curve presents fits to the ASPERA-3 observations on the MEX orbits.
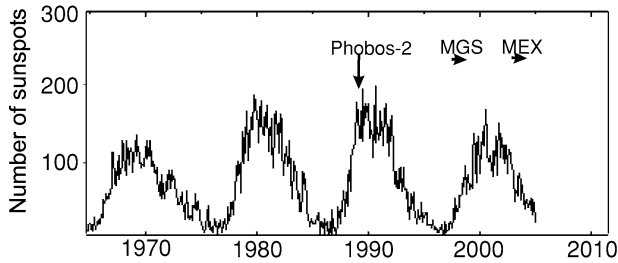

Figure 6. Solar cycle variations during the periods when the PHOBOS-2, MGS and MEX observations discussed in this paper were made.

The used equation of the MPB surface (in assumption of a cylindrical symmetry along the X-axis) in polar coordinates was (Vignes *et al.*, 2000)

$$r = \frac{L}{1 + \epsilon \cos \theta}. \tag{1}$$

Here $L = 0.96 R_M$ and $\epsilon = 0.9$ are the semi-latus tectum and the eccentricity, respectively. Polar coordinates (r, θ) are measured about the focus located at the point
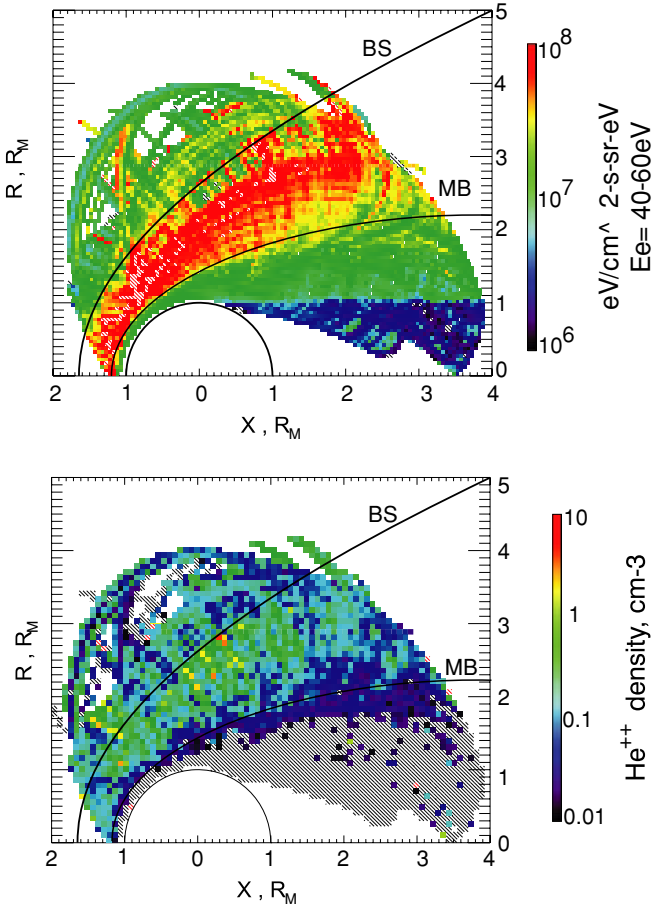
Figure 7. Images of fluxes of electrons ($E_e = 40$–$60\,\mathrm{eV}$) and density of He^{++} ions in cylindrical coordinates plotted on the total of the MEX orbits during 2004–2005. Positions of the MB (the MEX data) and bow shock (BS) are also given.

($x_0 = 0.78, 0, 0$). A better agreement with the MEX-ASPERA-3 observations, in particularly, at small solar zenith angles can be obtained by using the same values for L and ϵ, but moving the focus to $x_0 = 0.7$ (the green curve in Figure 5).

Figure 5 also shows that a scatter of the data points with respect to the nominal boundary position, increases with the solar zenith angle.

The boundary determined from a drop of the magnetosheath electrons coincides with a boundary of a "stoppage" of the solar wind. Figure 7 compares the median distributions of fluxes of the $E_e = 40$–$60\,\mathrm{eV}$ electrons and the number densities of He^{++} ions. The data set contains the measurements carried out by ASPERA-3 over two years (2004–2005). The magnetosphere almost void of solar wind particles can well be seen. Since the magnetic pile up boundary is also characterized by a drop of the magnetosheath electrons, MPB is the magnetospheric, obstacle boundary

which determines the position of bow shock and plasma flow around Mars. We used here a term MB for definition of the magnetospheric boundary , because of the lack of the magnetic field measurements on MEX.

The existence of an extended magnetospheric cavity for median conditions does not imply that solar wind can not penetrate to closer altitudes above the planet. Magnetospheric "images" plotted for maximum values of fluxes and densities in each bin reveal a significant contraction of the magnetosphere (not shown here) for extreme conditions in the solar wind. Among the main factors which are expected to account for the observed variations of the boundary position are the solar wind dynamic pressure, local crustal magnetic field sources and orientation of the interplanetary electric field $-V_{\rm sw} \times B_{\rm IMF}$.

2.1.1. *Solar Wind Dynamic Pressure Dependence*

In this paper we use a MGS proxy for the solar wind RAM pressure monitoring. It is assumed that the solar wind dynamic pressure is balanced at the induced magnetospheric boundary (MPB) by the magnetic field pressure of the draped IMF tubes. The pileup of the magnetic field and formation of the induced magnetic barrier occurs over a short distance, that accounts for a sudden drop of the solar wind electron and proton fluxes. The magnetic field value remains approximately constant for several hundred km in the magnetic pile up region (MPR) (Crider *et al.*, 2003). On mapping orbits, the MGS spacecraft moves along a circular 0200-LT/1400-LT polar trajectory at the altitude of ~400 km, crossing the MPR in the northern hemisphere. Since the magnetic field at middle latitudes of the northern hemisphere is primarily of induced origin, we can use its value as a proxy for the magnetic field pressure which stops the solar wind, and readily infer a proxy value for the solar wind dynamic pressure (Spreiter and Stahara, 1992)

$$k P_{\rm dyn} \cos^2 \theta = \frac{B^2}{2\mu_o},$$

(2)

where $k \sim 0.88$ and θ is the solar zenith angle and the magnetic field B is measured on each MGS orbit on the dayside at the reference point $\theta \sim 45°$. This proxy solar wind dynamic pressure $P_{\rm dyn}$ is adjusted to the times of the magnetospheric boundary crossings. It is worth noting that Vennerstrom *et al.* (2003) and Crider *et al.* (2003) have also successfully used the MGS data as a proxy for solar wind pressure. Brain *et al.* (2005) have shown that MGS was outside of the MPR, in the magnetosheath as much as 20–25% of the time during mapping orbits. For these orbits, the inferred RAM pressure is likely even higher than predicted by this method.

Figure 8 compares variations of the inferred solar wind dynamic pressure and the ratio $r_{\rm obs}/r_{\rm ave}$ which characterizes the difference in the measured and averaged boundary positions. Here $r_{\rm obs}$ is the length of the radius-vector between the focus point $(x_o, 0, 0)$ and the observation point of the MB, and $r_{\rm ave}$ is the distance from
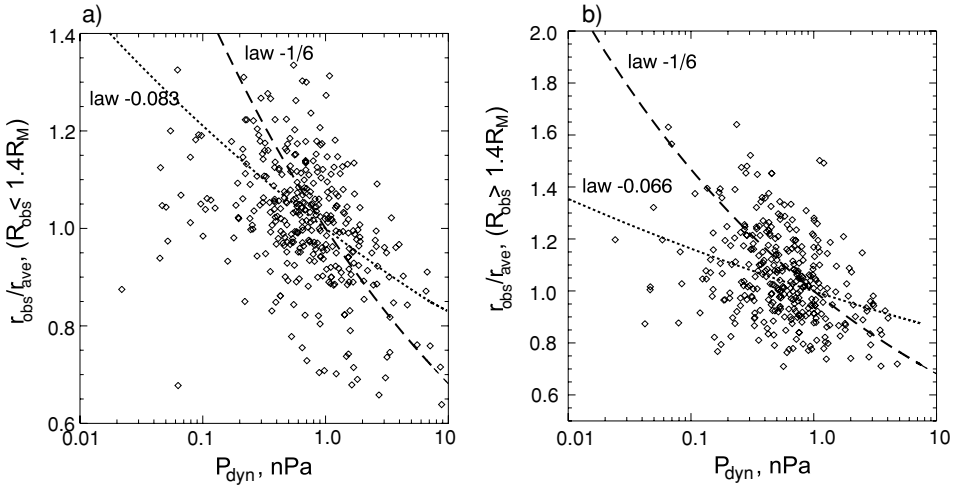
Figure 8. Variations in the MB positions as a function of the solar wind RAM pressure. The data are separated on two groups, $R < 1.4R_M$ (a) and $R > 1.4R_M$ (b), where R is a radial distance from the X-axis to the MB crossings. Dashed curves are the power law $P_{sw}^{-1/6}$ dependence. Dotted curves are the power law fits.

the focus to the crossing point of the average boundary surface and the vector r_{obs}. The MEX data are separated on two groups of $R_{obs} > 1.4R_M$ and $R_{obs} < 1.4R_M$, where R_{obs} is the radial distance from the X-axis to the observation point. The small $R_{obs} < 1.4R_M$ group corresponds to solar zenith angles less than 60–70°. It is observed that the response of the boundary position to the RAM pressure is better visible at smaller zenith angles. If the MB is asymmetrically shaped as suggested by Crider *et al.* (2004) and Brain *et al.* (2005), then at high SZA there should be larger scatter about the mean position of the boundary – making difficult to see the effects of pressure.

The dashed curves in Figure 8 show a power law ($P_{dyn}^{-1/6}$) dependence. Verigin *et al.* (1993) have shown that the diameter of the Martian tail D is proportional to $P_{dyn}^{-1/6}$ what is expected if Mars would have an intrinsic magnetosphere. A similar dependence was noted by Dubinin *et al.* (1996) although the authors have argued in favor of an induced magnetosphere. For the small R_{obs} group a power law fit is given by $r_{obs}/r_{ave} \sim P_{dyn}^{-0.053}$ that is in a good agreement with the MGS data, $k = -0.0546$ (Crider *et al.*, 2003). If we exclude the data points for small values of the RAM pressure ($P_{dyn} > 0.133$ nPa) then the power law index $k \sim -0.083$ (the dotted curve in Figure 8a). For the large R_{obs} group, the index $k = -0.065$ (the dotted curve in Figure 8b).

Thus the MEX data as well as the MGS observations show a weaker dependence between the RAM pressure and variations in the MB location than it is expected for a magnetic dipole obstacle. Nevertheless a power law dependence is still revealed.
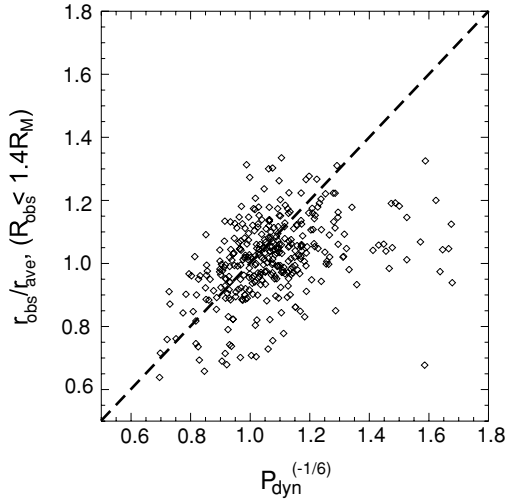
Figure 9. Variations in the MB position as a function of $P_{sw}^{-1/6}$.

Such dependence becomes weaker and ceases for small P_{dyn} that is better seen in Figure 9 which depicts the r_{obs}/r_{ave} as a function of $P_{dyn}^{-1/6}$.

It is worth noting that although an induced origin of the obstacle to solar wind at Mars is well established now, a question whether or not a power law dependence exists, remains important and is closely related to a question what makes an induced magnetosphere. An induced magnetosphere can be created by induction currents flowing in a conductive ionosphere or within the bodies (e.g. in molten cores) (see, for example, Luhmann *et al.*, 2004). Two types of induction mechanisms are usually considered, an unipolar induction where the current is driven by the $-V_{sw} \times B_{IMF}$ electric field or a classical electromagnetic induction associated with temporal variations (in direction or value) of the external magnetic field. Here, in a case of a unipolar induction, we do not separate unipolar currents flowing in a conducting body from currents flowing in a mass-loaded plasma (in both cases, currents are driven by the motional electric field). It has been shown that both types of induction may contribute to induced magnetic fields (Podgorny *et al.*, 1982). Temporal variations of the IMF induce a dipole magnetic field due to the currents in a conducting ionosphere (or/and interior), and a power-law dependence with index $k = -1/6$ of the boundary position as a function of solar wind dynamic pressure seems not to be unreasonable. Indeed, Brecht (1995) have observed a such dependence of the magnetotail width on the RAM pressure in hybrid simulations of the solar wind interaction with a "conducting" body. On the other hand, unipolar currents which bound the draped IMF induce a weakly dependent on a distance magnetic field (similar as the magnetic field within a solenoid). The observations of a weak power-law dependence show that both mechanisms probably contribute to the induced magnetic field at Mars.

While comparing the Phobos-2 and MGS, MEX observations it is also necessary to recall that solar wind pressure in the Phobos-2 data has been measured in-situ. On the other hand, the sampling was poorer.

2.1.2. *Interplanetary Electric Field Dependence*

For the study of the solar wind interaction with planets like Mars or Venus having draped magnetospheric configurations, the IMF reference frame is the most natural one. This coordinate system has the X^*-axis antiparallel with the upstream solar wind flow and Y^*-axis along the cross-flow magnetic field component of the IMF. Then the motional electric field $-V_{sw} \times B_{IMF}$ is always along the Z^*-axis. Since there is no magnetometer on the MEX spacecraft the only way to infer an information about the IMF is the MGS observations in the MPR. IMF directions have been previously derived from MGS data by Crider *et al.* (2001) for aerobraking data and by Brain *et al.* (2006) for mapping orbits. Assuming that the clock-angle of the IMF is not changed while the field lines are draped around Mars we can infer a proxy direction of the cross-flow magnetic field component and construct the IMF coordinate system. We used the same reference point in the dayside northern hemisphere as for the determination of a proxy RAM pressure. As a matter of fact, the IMF system is inadequate to observe simultaneously in two dimensions a possible "north-south" asymmetry due to the motional electric field and a "dawn-dusk" draping asymmetry, if different B_x polarities of the IMF for the same sector polarities are analyzed. Moore *et al.* (1990) have used a combination of rotations and foldings (see also Dubinin *et al.*, 1996). However, in our case, the lack of information about the X-component of the IMF does not allow to apply such foldings.

Normalizing a boundary position to average solar wind conditions ($P_{dyn} = 1$ nPa) by using the power law fit dependence we can test a possible asymmetry of the magnetosphere in the IMF coordinate plane. Figure 10 shows r_{obs}/r_{ave} in the plane Y^*Z^*. We observe only a certain elongation of the magnetospheric shape in the "north-dawn" direction for $R_{obs} > 1.4 R_M$ probably caused by two factors: (i) a preferential pile up of the IMF in the "northern" hemisphere and (ii) a "dawn-dusk" asymmetry of the draping due to X-component of the IMF. It will be shown subsequently that a similar trend is observed in the distribution of CO_2 photoelectrons. It is worth noting that draping directions in the subsolar region and in the reference point at the middle latitudes of the northern hemisphere which was used to infer the IMF direction may be somewhat different due to 'weathervaning' effects (see e.g. Brain *et al.*, 2006). Then the overall pattern must be rotated clockwise at ~ 30–$40°$ and a 'north-south' asymmetry related to the motional electric field will be better noticeable.

Observations near Venus have shown that the piled up magnetic field is stronger in the Z^*-hemisphere into which the motional electric field is pointing (Luhmann *et al.*, 1985). A similar effect is found at Mars (Vennerstrom *et al.*, 2003) as well as in 3-D hybrid simulations of the solar wind interaction with Mars (Bößwetter *et al.*, 2004; Modolo *et al.*, 2005). Therefore it is might be expected that the position of the
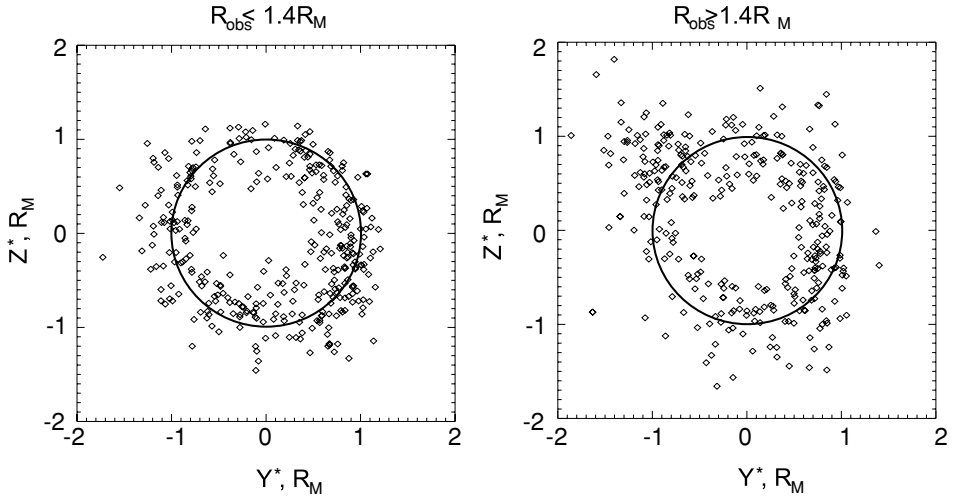
Figure 10. Variations in the MB position in the Y^*Z^*-plane, where the Y^*-axis is along the cross-flow component of the IMF, and Z^*-axis is along the motional electric field in the solar wind.

magnetospheric boundary is further from the planet in the $+Z^*$-hemisphere where mass-loading effects could be more essential (Dubinin *et al.*, 1998). On the other hand, effects of a finite proton Larmour radius can lead to an opposite asymmetry (Brecht, 1997; Bößwetter *et al.*, 2004). Further observations are necessary for better understanding of different controlling factors which interfere the general pattern of the Martian magnetosphere.

2.1.3. *Crustal Field Dependence*
The crustal magnetic fields can also influence the position of the magnetospheric boundary as the magnetic pressure in some localized regions may be high enough to balance the solar wind dynamic pressure. Crider *et al.* (2002) have found that the MPB distance increases with increasing southern latitude. Using the electron measurements by ASPERA-3-ELS, Fraenz *et al.* (2006a) have shown that the altitude of the intruded magnetosheath electrons ($E_e = 80\text{–}100\,\text{eV}$) increases with the strength of the crustal field. Figure 11a shows a relative shift of the boundary in the dayside southern hemisphere with respect to its averaged position ($r_{\text{obs}}/r_{\text{ave}}$) as a function of the strength of the crustal magnetic field. We used the crustal field strength interpolated on a regular grid for an altitude of $400\,\text{km}$ from the MGS MAG/ER observations as presented by Connerney *et al.* (2001). Although the sampling of measurements above the strong crustal sources is small an upward motion of the boundary with increasing magnetic field strength is clearly observed. There is a reasonable agreement with the picture of the intrusion of magnetosheath electrons as a function of crustal field strength (Figure 11b).
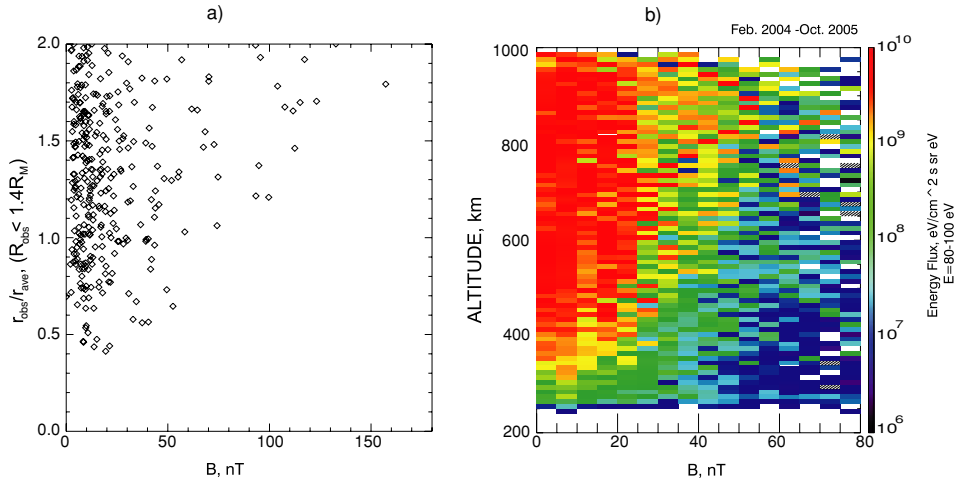
Figure 11. (a) Variations in the MB position in the southern dayside hemisphere as a function of the strength of the crustal magnetic field at 400 km. (b) Maximum fluxes of the electrons with $E_e = 80$–100 eV observed at different altitudes during the MEX observations (Feb 2004–Oct 2005) on the dayside as a function of the magnetic field strength of the crustal sources at altitude of 400 km.

2.2. IONOSPHERIC PHOTOELECTRONS

The ionospheric electrons are well traced by the peaks in the energy spectra of the electrons in the range of 20–30 eV. Observations of such electrons can be used to probe the Martian ionosphere. Figure 12 shows the distribution of the energy flux of CO_2 – photoelectrons in the energy range ($\delta E = 4$ eV) centered near its characteristic "spectral lines" (20–30 eV) in cylindrical coordinates. Floating of these spectral peaks due to spacecraft potential variations was taken into account. The ionospheric electrons are observed at altitudes up to ~7000 km. Statistics of their occurrence at different altitudes is discussed in more detail by Frahm *et al.* (2006b). Another interesting feature is that the photoelectrons are often detected close to the nominal magnetospheric boundary almost filling the whole dayside magnetosphere. In many cases the photoelectrons are also observed close to the distant positions of the magnetospheric boundary. These features probably imply an important role of the ionospheric plasma as an obstacle to solar wind.

Figure 13 shows the radial distance of the MB crossings versus the highest radial distance at which ASPERA-3 records the photoelectrons. It is observed that a gap between the MB and PEB can be rather small even at large distances from Mars. Unsolved yet is the question, does a drop of photoelectrons (PEB) near the magnetospheric boundary (MB/MPB) correspond to the ionopause (if we speak in terms of pressure balance)?

According to the MGS aerobraking observations (Mitchell *et al.*, 2000), at solar zenith angles (SZAs) ~80°, the transition from the region occupied by the shocked
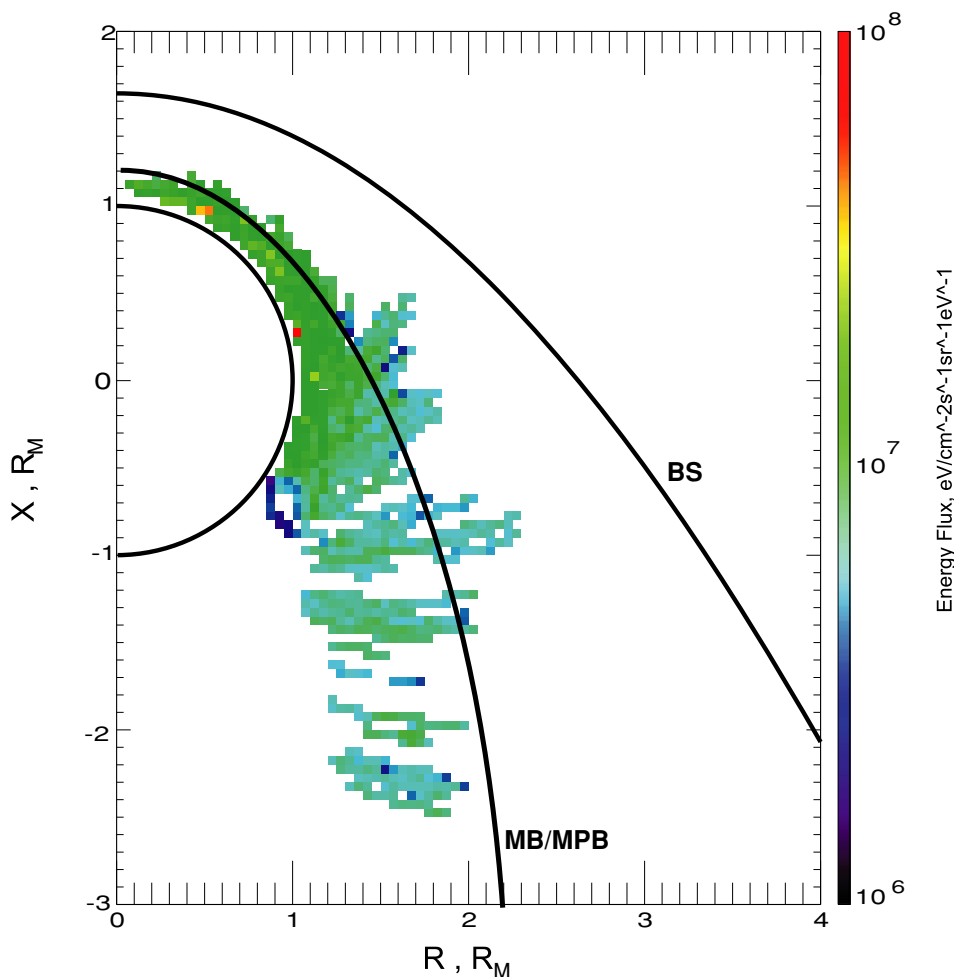
Figure 12. Regions in cylindrical coordinates $R - X$ where CO_2-photoelectrons were observed. The color shows the energy flux of the photoelectrons.

solar wind electrons to the ionosphere characterized by the appearance of Auger electrons ($\sim$500) eV and poorly resolved photoionization peaks at 20–50 eV occurs in the altitude range 180–800 km with a median value of 380 km. The electron spectrometer (ELS) of the ASPERA-3 experiment due to a higher energy resolution was able to identify the boundary of photoelectrons with a better accuracy as a position where fluxes of CO_2-photoelectrons cease. It is shown that a drop of the magnetosheath electrons ($E_e = 100$ eV) on the dayside approximately coincides with MB and there is a clear gap between MB and PEB.

To date reliable ionospheric profiles near the MB/MPB are absent. Recent MARSIS ionospheric soundings performed on MEX have shown that the
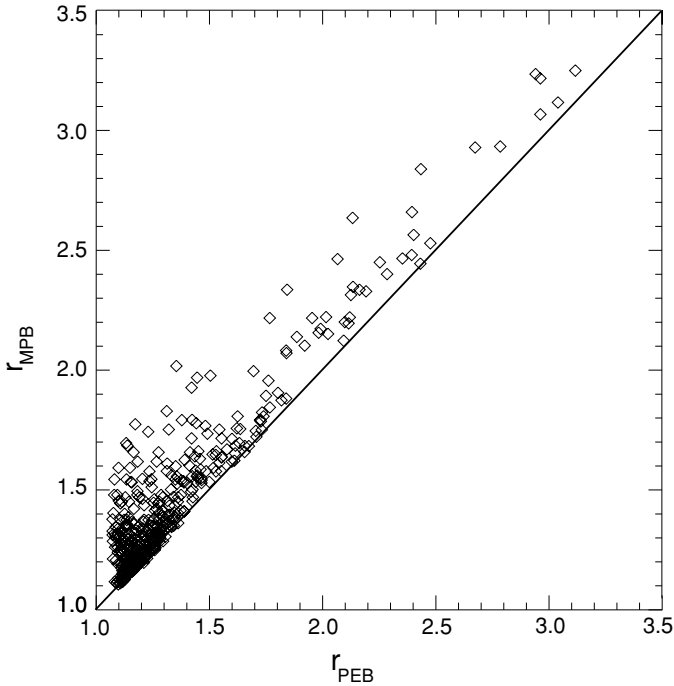
Figure 13. Positions of the MB and PEB (the radial distances from Mars) for the orbits at which both boundaries were observed.

ionospheric number density at altitude of $\sim$400 km near the terminator is about of 3×10^3 cm^{-3} (Gurnett *et al.*, 2005). This implies a possible essential ionospheric contribution to the pressure balance at altitudes of the magnetospheric boundary. However, it is unlikely that the ionospheric pressure at PEB altitudes is able to stop the solar wind. We may assume that some part of the momentum of the solar wind can be transferred to the ionosphere via the magnetic field stresses driving the ionospheric plasma into the bulk motion. This motion can explain the observations of ionospheric photoelectrons far in the tail. The photoelectrons can also lift up along the magnetic field lines and, particularly, along the reconnected crustal field lines which are stretched into the tail ("polar wind" at Mars). The existence of field-aligned fluxes of photoelectrons in the $+Z^*$ hemisphere at the negative Y^* values can be tentatively observed in Figure 14 which presents the fluxes of CO_2-photoelectrons in the IMF coordinate system. However, since photoelectron fluxes are mainly contained within the magnetospheric cavity a bulk transport is likely a dominant process. A small bulge in the $(-Y^* + Z^*)$ – hemisphere is similar to a bulge in the position of the magnetospheric boundary (Figure 10) implying a contribution of the ionospheric plasma to the formation of the obstacle. The observed "dawn-dusk" asymmetry can be caused by different tension forces of the draped field lines due to the presence of the X-component of the IMF. Since the motion of
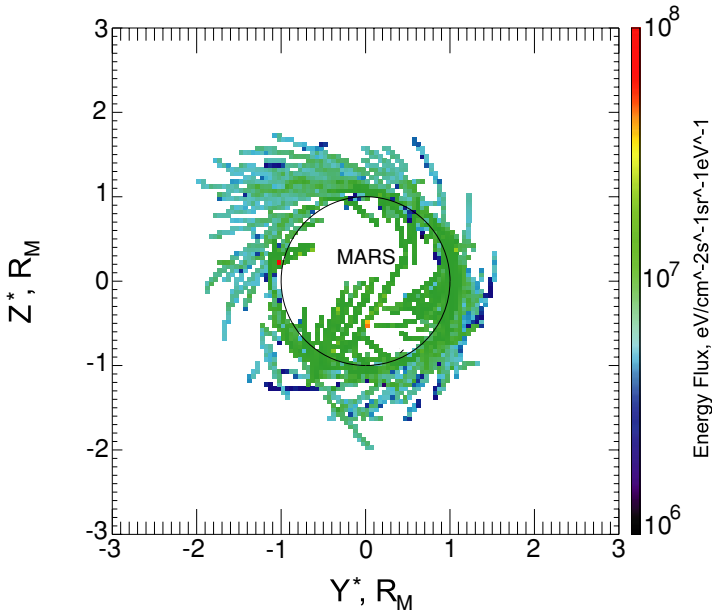
Figure 14. Regions in the IMF Y^*Z^* plane where CO_2-photoelectrons were observed. The same dataset as in Figure 13 is presented.

low-energy ionospheric plasma is not quantified yet it is difficult to estimate escape fluxes of oxygen from the topside ionosphere.

2.3. RAY STRUCTURE NEAR THE WAKE BOUNDARY

The ASPERA-3 experiment has often observed a spatially narrow structure composed of hot sheath-like electrons and planetary ions near the wake boundary (see the second and third panels in Figure 1 and Dubinin *et al*., 2006b). The structure appears near the terminator plane and is stretched, like a ray into the tail. Figure 15a shows in $R - X$ coordinates locations of the events observed in 2004. Figure 15b gives the image of electron fluxes in the energy range of 80–100 eV along the orbits on which ray-electron structures were observed. Such rays are important erosion channels through which planetary ions are transported to the tail. That can be readily inferred from Figure 15c which shows density fluxes of oxygen ions along the same set of MEX orbits. It was suggested (Dubinin *et al*., 2006b) that draped field lines slipping along the magnetospheric surface near the MPB, around the "magnetic poles" can push planetary ions into the magnetosphere. This mechanism also explains the formation of the plasma sheet which separates two magnetic field lobes in the induced tail. Recent hybrid simulations (Bößwetter *et al*., 2004; Modolo *et al*., 2005) have shown a distinct asymmetry in the strength of the field
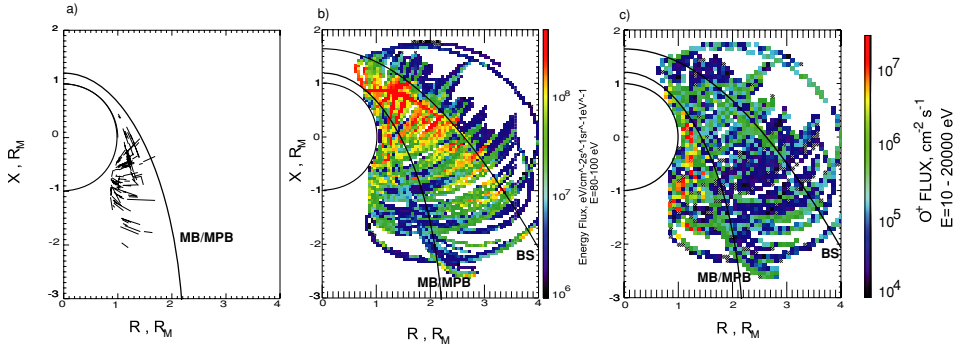
Figure 15. (a) Orbital segments in cylindrical coordinates at which electron signatures of the ray-like structures near the wake boundary were observed. (b) The fluxes of electrons with $E_e = 80–100\,\mathrm{eV}$ measured on the same set of orbits on which ray structures were detected. (c) Fluxes of oxygen ions on these orbits. The positions of the bow shock (BS) and magnetospheric boundary (MB) respectively inferred from the MGS and MEX observations are also shown.
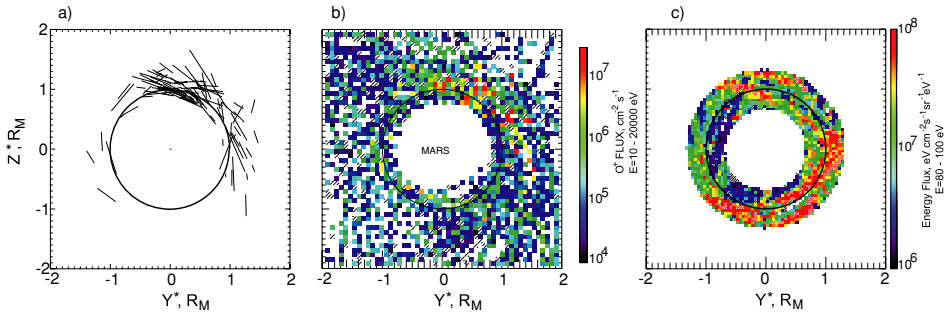

Figure 16. (a) Orbital segments in the Y^*Z^*-plane of the IMF coordinate system at which the electron signatures of ray-like structures near the wake boundary were observed. (b) the fluxes of oxygen ions along these MEX trajectories transformed into the IMF reference frame. (c) Maximum fluxes of 80–100 eV electrons in the bins of the ring-area $0.7–1.3R_M$ around Mars for two year observations.

at the MPB. The maximum intensity of the draped magnetic field is observed in the hemisphere into which the motional electric field is pointing (the "northern" hemisphere in the IMF coordinate system). Therefore, if this mechanism works, one would expect a preferential observation of ray structures in the $+Z^*$ hemisphere near the pole. Figure 16a depicts the locations of the orbital segments along which ray-events were observed in the IMF Y^*Z^*-plane. It is seen that most of the events are clustered near the "northern magnetic pole." There are also events near the "magnetic equator" which could be the counterparts of stretched ray-like structures in the "magnetic equatorial plane" observed in 3D-hybrid simulations (Bößwetter *et al.*, 2004; Modolo *et al.*, 2005). A force which pushes planetary ions along the field lines is probably a day-night thermal pressure gradient. The asymmetry of ray structures is also revealed on the right panel in Figure 16b which shows the

fluxes of oxygen ions along the orbits in which the ray features were observed in the electron data.

Another mechanism which associates the events with auroral inverted "V" structures suggests their appearance in the southern hemisphere where the shear flows at the boundary of open, draped IMF field lines and closed field lines from crustal sources can generate field-aligned currents and the parallel electric fields (Lundin *et al.*, 2006). Figure 16c depicts the maximum fluxes of the 80–100 eV electrons in the ring-area within 0.7–$1.3 R_M$ of the Mars-Sun line at $X < 0$ during two years. The fluxes near wake boundary dominate in the southern hemisphere. Thus both mechanisms probably contribute to the occurrence of ray-like structures.

2.4. BOUNDARY LAYER AND PLASMA SHEET

Another important reservoir of planetary ions is the boundary layer. The existence of the boundary layer/mantle in the Martian magnetosphere has been shown during the first Soviet space missions to Mars (Vaisberg, 1992) as well as in the Phobos-2 observations (Lundin *et al.*, 1990a; Breus *et al.*, 1991; Dubinin *et al.*, 1996). Moreover, it was assumed that the boundary layer is a main channel for the escape of planetary ions (Lundin *et al.*, 1990b). Figure 17 (left panel) shows in the $R - X$ plane the orbital segments near the MB along which planetary ions were detected. The right panel depicts the values of oxygen ion fluxes measured during these intervals. The main fluxes are observed within the magnetosphere although on some orbits remarkable fluxes of planetary ions were also recorded in the
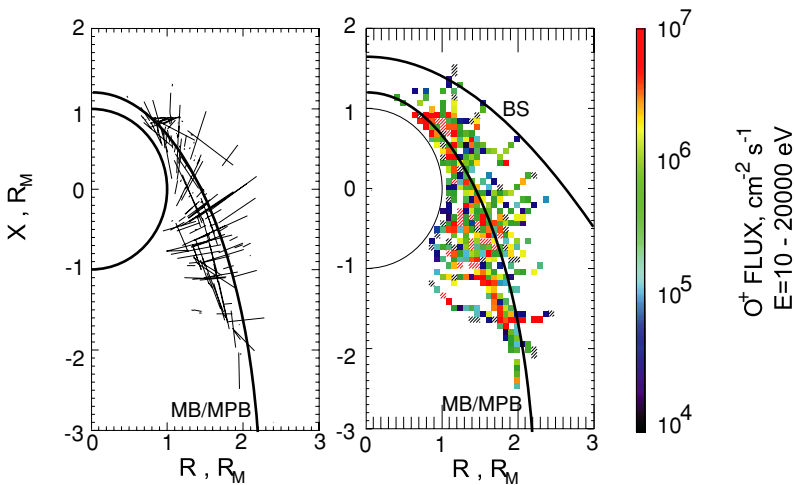

Figure 17. (a) Orbital segments in the cylindrical coordinates at which the fluxes of planetary ions were detected in the boundary layer/mantle. The right panel shows the values of oxygen fluxes measured during these intervals. The positions of the bow shock (BS) and magnetospheric boundary (MB) respectively inferred from the MGS and MEX observations are also shown.
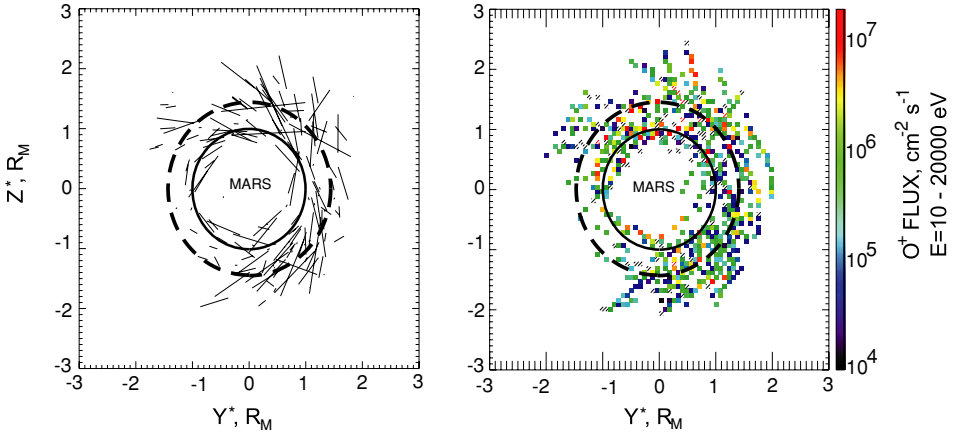
Figure 18. Orbital segments in the Y^*Z^*-plane of the IMF coordinate system at which the signatures of the boundary layer were found. The right panel depicts the fluxes of oxygen ions along these orbital intervals. Dashed circle depicts the nominal location of the MB in the terminator plane.

adjacent magnetosheath. The values of fluxes in the boundary layer often exceed $10^7 \, \text{cm}^{-2} \, \text{s}^{-1}$.

The geometry of the outflowing plasma is very important for calculations of the total escape rate of planetary matter. Analyzing the ASPERA data on Phobos-2 Lundin *et al.* (1989, 1990b) have suggested that a primary solar wind induced escape with a total rate of about $2.5 \times 10^{25} \, \text{s}^{-1}$ occurs through a cylindrically symmetric boundary layer. Verigin *et al.* (1991) have made the assumption that the main channel for the loss of planetary ions is the plasma sheet. Correspondingly, the estimated total outflow rate in this case is significantly less ($\sim 5 \times 10^{24} \, \text{s}^{-1}$). Figure 18 presents the data set of the observations made in the boundary layer with ASPERA-3 on MEX in the IMF coordinate system. A strong "dawn-dusk" asymmetry is probably related with the different draping features due the X-component of the IMF. If we assume that planetary oxygen ions emanate from an asymmetric ring-shaped area $0.8R_M$ in thickness around the terminator and typical fluxes of ions are of the order of $\sim 10^6$–$10^7 \, \text{cm}^{-2} \, \text{s}^{-1}$, the total escape rate would be about 6×10^{23}–$6 \times 10^{24} \, \text{s}^{-1}$. These estimates rather correspond to the maximum escape fluxes since the boundary layer was observed only in ~ 20–25% of the orbits. The absence of the boundary layer in ~ 80% of cases implies that there are probably other, unknown yet factors, than the geometry of the IMF, which control the escape processes. Recall here, that the MEX measurements were carried out close to solar minimum conditions while the Phobos-2 spacecraft has operated near Mars at solar maximum when the oxygen exosphere was expected to be denser.

It was observed (see Section 1) that on some orbits the boundary layer is characterized by a sudden additional heating of magnetosheath electrons. Spectra of electrons in these cases become similar to the spectra observed in ray-structures
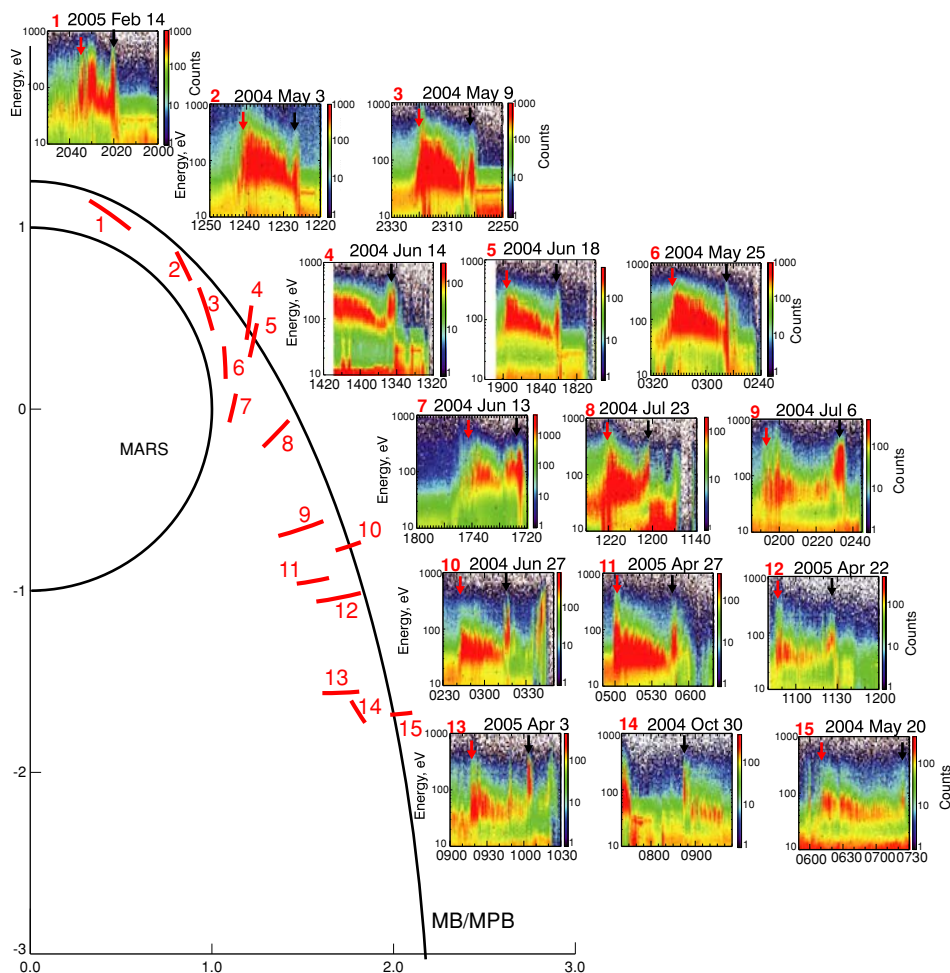
Figure 19. Sites near the inner boundary of the magnetosheath where the sheath electrons inhibit an additional heating. The spectrograms of electron fluxes which display these events are shown on the small right panels. Red and black arrows show the positions of the bow shock and boundary events (BE), respectively.

or in the plasma sheet. The ion composition is dominated by O^+ and O_2^+ ions. A change of ion composition of the plasma within these structures implies that the observed spikes of heated electrons at the inner edge of the sheath are not related to temporal variations in the magnetosheath caused by the passage of different types of inhomogeneities and discontinuities in the solar wind, but that they are an inherent boundary layer feature. Figure 19 shows the position of sample events in cylindrical coordinates. The corresponding spectrograms of electron fluxes with clear spikes of electron heating near the MB are also shown. The inner part of the magnetosphere is readily recognized by the absence of magnetosheath-like electrons. The positions of

the bow shock (BS) and the boundary events (BE) are also marked by red and black arrows, respectively. In IMF coordinates the BEs appear in the $+Z^*$-hemisphere. More analysis is required to understand the origin of these events.

The magnetosphere structure within the optical shadow of Mars ($R < 1R_M$) is still poorly covered by the ASPERA-3 measurements. The observations of the plasma sheet carried out in 2004 yield a similar morphological pattern as for the ray-structures (see Figures 15 and 16) which may imply that they have a common root. The values of oxygen fluxes in the plasma sheet are somewhat higher than in the boundary layer and often exceed $10^7\,\mathrm{cm}^{-2}\,\mathrm{s}^{-1}$. Fedorov *et al.* (2006) have also distinguish two different escape channels for planetary ions, a layer adjacent to the MB/MPB and the planetary shadow. Authors showed that mechanisms of ion acceleration in the boundary layer and wake can be different and controlled by the IMF direction.

3. Summary

We explored the morphology of the main plasma regions and their boundaries by analyzing MEX ASPERA-3 data collected in 2004.

1. It is shown that a magnetospheric cavity strongly depleted in solar wind particles is formed. The position of its boundary determined by a drop of fluxes of ~50 eV magnetosheath electrons coincides with a boundary determined by a drop of solar wind ions. This implies that the magnetospheric boundary is collocated with the MPB which is also characterized by a drop of the magnetosheath electrons.
2. We have analyzed the position of the magnetospheric boundary and compared it with Phobos-2 and MGS observations. Good agreement with Phobos-2 observations at small solar zenith angles and with MGS data for larger angles is observed. A general reasonable agreement in the MB position observed at different phases of solar activity implies that it is not sensitive to this parameter. A similar conclusion was made by Vignes *et al.* (2000) while comparing the Phobos-2 and MGS data.
3. Variations in the MB location increase with increasing SZA.
4. We have analyzed the dependence of MB locations on solar wind dynamic pressure. We used a MGS proxy for solar wind RAM pressure assuming that the RAM pressure is balanced at the MPB by the magnetic field pressure. It is generally observed that variations of the MB position are in a reasonable agreement with a magnetic origin of the obstacle to the solar wind (an obstacle formed by a barrier of the piled up IMF field lines). It is shown that a response of the MB to the RAM pressure is revealed more clearly at SZA $\leq 60°$–$70°$. The K–H instability of shear flows near the MB may result in large inward-outward

motions of the MB at larger zenith angles providing a significant "scattering" in the MB locations.

5. The ASPERA-3 data show a weaker power law dependence between the RAM pressure and variations in the MB location than can be expected for the magnetosphere created only by currents of the electromagnetic induction.

6. In the IMF coordinate system, determined by the cross-flow component of the IMF, a "north-south" asymmetry in the MB location caused by mass loading effect in the electric field pointing hemisphere is only revealed if a weather-vaning of the draped field lines is taken into account while inferring the IMF direction.

7. Although the sampling of MB measurements above strong crustal source is poor, an upward lift of the MB is observed. This trend is also confirmed by an altitude-crustal field dependence of protrusion of magnetosheath electrons.

8. Ionospheric photoelectrons traced by their characteristic peaks in energy spectra are used to identify the photoelectron boundary PEB and explore their distribution within the Martian magnetosphere. Photoelectrons can be observed close to the MB locations implying an important role of the ionospheric component in dynamic processes responsible for the formation of the magnetospheric obstacle at Mars. It is unlikely that PEB and ionopause (as a pressure balance boundary) are collocated. It is assumed that some part of the momentum from solar wind is transferred to the ionosphere driving it into a convective motion. This motion together with a mechanism of "polar wind" along "open" field lines can explain the observation of ionospheric photoelectrons at distances more than $3R_M$ far in the tail.

9. In the IMF reference frame the distribution of photoelectrons reveals a similar asymmetry as the magnetospheric boundary.

10. It is shown that the position of ray-like structures centered close to the wake boundary are governed by the IMF direction. The events are clustered in the hemisphere of locally upward convective electric field. This supports the suggestion that these structures are formed in a process of scavenging of planetary plasma by draped magnetic field lines near the "magnetic poles." However their dominance in the southern hemisphere also implies a possible important role of auroral-like acceleration processes at Mars. A "dawn-dusk" asymmetry due to draping features is also revealed.

11. It is shown that the boundary layer/mantle is an important channel for planetary ions escaping from the Martian space. A strong "dawn-dusk" asymmetry in IMF coordinates appeared due to a draping asymmetry. Estimates of outflowing fluxes of oxygen ions yield $6 \times 10^{23} - 6 \times 10^{24}$ s^{-1}. However, these values may be somewhat revised after the final instrumental calibration.

12. If PEB is not a boundary at which the solar wind pressure is balanced by the thermal pressure of the cold ionospheric plasma then plasmas of ionospheric and atmospheric origin which fill the region between MB and ionopause must be driven into a convective motion.

13. An interesting class of events is observed close to the inner boundary of the magnetosheath. These boundary events are characterized by an abrupt additional heating of magnetosheath electrons and remarkable fluxes of planetary ions. It is not clear yet whether such events are the manifestation of a transition, "viscous-like" layer as observed near Venus or crossings of a plasma sheet near the MB.

Acknowledgements

References

Acuña, M. H., Connerney, J., and Wasilewski, P., *et al*.: 1998, *Science* **279**, 5357, 1676.
Barabash, S., Lundin, R., Andersson H., *et al*.: 2004, *ESA Publication* **SP-1240**, 121.
Bertucci, C., Mazelle, C., Crider D., *et al*.: 2003, *Geophys. Res. Lett*. **30**, 1876, doi:10.1029/2002GL015713.
Bößwetter, A., Bagdonat, T., Motschmann, U., and Sauer, K.: 2004, *Annal. Geophys*. **22**, 4363.
Brace, L. H., Kasprzak, W. T., Taylor, H. A., Theis, T. F., Russell, C. T., Barnes, A. *et al*.: 1987, *J. Geophys. Res*. **92**, 15.
Brain, D. A., Bagenal, F., Acuña, M., and Connerney, J. E.: 2003, *J. Geophys. Res*. **108**, 1424, doi:10.1029/2002JA009482.
Brain, D. A., Halekas, J. S., Lillis, R. J., Mitchell, D. L., Lin, R. P., and Crider, D. H.: 2005, *Geophys. Res. Lett*. **32**, 18, doi: 10.1029/2005GL023126. L18203.
Brain, D. A., Mitchell, D. L., and Halekas, J. S.: 2006, *Icarus* **182**, 464.
Brecht, S. H.: 1995, *Geophys. Res. Lett*. **22**, 1181.
Brecht, S. H.: 1997, *J. Geophys. Res*. **102**, 4743.
Breus, T., Krymskii, A., Lundin, R. , Dubinin E., *et al*.: 1991, *J. Geophys. Res*. **96**, 11165.
Connerney, L. E., Acuña, M. ,Wasilewski, P., Kletetschka, G., Ness, N. F., Reme, H. *et al*.: 2001, *Geophys. Res. Lett*. **28**, 4015.
Crider, D. H.: 2001, *Adv. Space Res*. **27**, 1831.
Crider, D. H.: 2004, *Adv. Space Res*. **33**, 152.
Crider, D. H., Vignes, D., Krymskii, A., Breus, T., Ness, N., Mitchell, D. *et al*.: 2003, *J. Geophys. Res*. **108**, 1461, doi:10.1029/2003JA009875.

Dubinin, E., Lundin, R., Riedler, W., Schwingenschuh, K., Luhmann, J., Russell, C. T. *et al*.: 1991, *J. Geophys. Res.* **96**, 11189.

Dubinin, E., Lundin, R., Koskinen, H., and Pissarenko, N.: 1993, *J. Geophys. Res.* **98**, 3991.

Dubinin, E., Lundin, R., and Schwingenschuh, K.: 1994, *J. Geophys. Res.* **99**, 21233.

Dubinin, E., Sauer, K., Lundin, R., Norberg, O., Trotignon, J.-G., Schwingenschuh, K. *et al*.: 1996, *J. Geophys. Res.* **101**, 27061.

Dubinin, E., Sauer, K., Delva, M., and Tanaka, T.: 1998, *Earth Planets Space* **50**, 873.

Dubinin, E., Winningham, J. D., Fraenz, M., Woch, J., *et al*.: 2006a, *Icarus* **182**, 343.

Dubinin, E., Lundin, R., Fraenz, M., Woch, J., *et al*.: 2006a, *Icarus* **182**, 337.

Fraenz, M., Winningham, J. D., Dubinin, E., Roussos, E., *et al*.: 2006a, *Icarus* **182**, 406.

Fraenz, M., Dubinin, E., Roussos, E., Woch, J.: 2006b, *Space Sci. Rev.*, this volume, doi: 10.1007/s11214-006-9115-9.

Frahm, R., Winningham, J. D., Sharber, J. R., *et al*.: 2006a, *Icarus* **182**, 371.

Frahm, R., Winningham, J. D., Sharber J. R., *et al*.: 2006b, *Space Sci. Rev.*, this volume, doi: 10.1007/s11214-006-9119-5.

Gurnett, D. A., Kirchner, D. L., Huff, R. L., Morgan, D., *et al*.:2005, *Science* **310**, 1929.

Hanson, W. B., Sanatani, S., and Zuccaro, D. R.: 1977, *J. Geophys. Res.* **82**, 4351.

Hanson, W. B., and Mantas, G. P.: 1988, *J. Geophys. Res.* **93**, 7538.

Harnett, E. M., and Winglee, R. M.: 2005, *J. Geophys. Res.* **110**, A07226, doi: 10.1029/2003JA010315.

Kliore, A. J.: 1992, in J. G. Luhmann, M. Tatrallyay, and R. O. Pepin, (eds.), *Venus and Mars: Atmospheres, Ionospheres and Solar Wind Interactions*, AGU monograph, **66**, Washington, DC, p. 265.

Luhmann, J. G., Russell, C. T., Spreiter, J. R., and Stahara, S. S.: 1985, *J. Geophys. Res.* **5**(4), 307.

Luhmann, J. G.: 1993, *Adv. Space Res.* **98**, 17615.

Lundin, R., and Dubinin, E.: 1992, *Adv. Space Res.* **12**(9), 255.

Lundin, R., Zakharov, A., Pellinen, R., *et al*.: 1989, *Nature* **341**, 609.

Lundin, R., Zakharov, A., Pellinen, R., *et al*.: 1990a, *Geophys. Res. Lett.* **17**, 873.

Lundin, R., Zakharov, A., Pellinen, R., *et al*.: 1990b, *Geophys. Res. Lett.* **17**, 877.

Lundin, R., Dubinin, E., Koskinen, H., Norberg, O., Pissarenko, N., and Barabash, S.: 1991, *Geophys. Res. Lett.* **18**, 1059.

Lundin, R., Barabash, S. , Andersson, H., *et al*.: 2004, *Science* **305**, 1933.

Lundin, R., Winningham, J. D., Barabash, S., *et al*.: 2006, *Science* **311**, 980.

Mantas, G. P., and Hanson, W. B.: 1979, *J. Geophys. Res.* **84**, 369.

Mazelle, C., Reme, H., Sauvaud, J.-A., D'Uston, C., and Carlson, C. W.: 1989, *Geophys. Res. Lett.* **16**, 1035.

Mitchell, D. L., Lin, R. P., Mazelle, C., *et al*.: 2001, *J. Geophys. Res.* **106**, 23419.

Modolo R., Chanteur, G., Dubinin, E., Matthews, A.: 2005, *Annal. Geophys.* **23**, 433.

Moore, K. R., McComas, D., Russell, C. T., and Mihalov, J. D.: 1990, *J. Geophys. Res.* **95**, 12005.

Nagy, A. F., Winterhalter, D., Sauer, K., *et al*.: 2004, *Space Sci. Rev.* **111**(1), 33.

Neubauer, F. M.: 1987, *Astron. Astrophys.* **187**(1–2), 73.

Pätzold, M., Tellmann, S., Häusler, B., Hinson, D., Schaa, R., and Tyler, G. L.: 2005, *Science* **310**, 837.

Pedersen, A., Nairn, C., Grard, R., and Schwingenschuh, K.: 1991, *J. Geophys. Res.* **96**, 11243.

Perez-de-Tejada, H.: 1979, *J. Geophys. Res.* **84**, 1555.

Perez-de-Tejada, H., Intriligator, D. S., and Strangeway, R. J.: 1993, *Geophys. Res. Lett.* **20**, 991.

Podgorny, I., Dubinin E., and Israelevich, P.: 1982, *Moon and Planets* **27**, 397.

Raeder, J., Neubauer, F., Ness, N. F., Burlaga, L. F.: 1987, *Astron. Astrophys.* **187**(1–2), 61.

Russell, C. T.: 1992, in J. G. Luhmann, M. Tatrallyay, and R. O. Pepin (eds.), *Venus and Mars: Atmospheres, Ionospheres and Solar Wind Interactions*, AGU monograph, **66**, Washington, DC, p. 225.

Slavin, J., Smith, E. J., Tsurutani, B. T., Siscoe, G. L., Jones, D. E., and Mendis, D. A.: 1986, *Geophys. Res. Lett.* **13**, 283.

Smith, E. J., Davis, L., Coleman, P. L., and Jones, D. E.: 1965, *Science* **149**, 1241.

Spenner, K., Knudsen, W. C., Miller, K. L., Novak, V., Russell C. T., and Elphic, R. C.: 1980, *J. Geophys. Res.* **85**, 7655.

Spreiter, J. R., and Stahara, S. S.: 1992, in J. G. Luhmann, M. Tatrallyay, R. O. Pepin, (eds.), *Venus and Mars: Atmospheres, Ionospheres and Solar Wind Interactions*, AGU Monograph, **66**, Washington, DC, p. 345.

Trotignon, J.-G., Dubinin, E., Grard, R., Barabash, S., and Lundin, *J. Geophys. Res.* **101**, 24965.

Vaisberg, O.: 1992, *Venus and Mars: Atmospheres, Ionospheres and Solar Wind Interactions*, in: J. G. Luhmann, M. Tatrallyay, R. O. Pepin, (eds.), AGU monograph, **66**, Washington, DC, p. 311.

Verigin, M., Shutte, N., Galeev, A., Gringauz, K. I., *et al*.: 1991, *Planet. Space Sci.* **39**, 131.

Verigin, M., *et al*.: 1993, *J. Geophys. Res.* **98**, 1303.

Vennerstrom, S. Olsen, N., Purucker, M., and Acuña, M.: 2003, *Geophys. Res. Lett.* **30**, 1369, doi:10.1029/2003GL016883.

Vignes. D., Mazelle, C., Reme, H., Acuña, M., *et al*.: 2000, *Geophys. Res. Lett.* **27**, 49.

Yeroshenko, Ye. Riedler, W. R., Schwingenschuh, K., Luhmann, J. G., Ong, M., and Russell, C. T.,: 1990, *Geophys. Res. Lett.* **17**, 885.

Zhang, T. L., Luhmann, J. G., and Russell, C. T.: 1991, *J. Geophys. Res.* **96**, 11145.